



HAL
open science

A general approach for brushed dc machines simulation using a dedicated field/circuit coupled method

Raphael Andreux, J. Fontchastagner, Nouredine Takorabet, Nicolas Labbe,
Jean-Sebastien Metral

► **To cite this version:**

Raphael Andreux, J. Fontchastagner, Nouredine Takorabet, Nicolas Labbe, Jean-Sebastien Metral.
A general approach for brushed dc machines simulation using a dedicated field/circuit coupled method.
Progress In Electromagnetics Research, 2014, 145 (5), pp.213 - 227. 10.2528/PIER14011402 . hal-01383620

HAL Id: hal-01383620

<https://hal.univ-lorraine.fr/hal-01383620v1>

Submitted on 8 Dec 2016

HAL is a multi-disciplinary open access archive for the deposit and dissemination of scientific research documents, whether they are published or not. The documents may come from teaching and research institutions in France or abroad, or from public or private research centers.

L'archive ouverte pluridisciplinaire **HAL**, est destinée au dépôt et à la diffusion de documents scientifiques de niveau recherche, publiés ou non, émanant des établissements d'enseignement et de recherche français ou étrangers, des laboratoires publics ou privés.

A General Approach for Brushed DC Machines Simulation Using a Dedicated Field/Circuit Coupled Method

Raphaël Andreux^{1, 2}, Julien Fontchastagner^{1, *}, Nouredine Takorabet¹,
Nicolas Labbe², and Jean-Sébastien Métral²

Abstract—This paper deals with the modeling of the brushed DC motor used as a reinforced starter for a micro-hybrid automotive application. The aim of such a system, also called “stop-start”, is to stop a combustion engine when the vehicle pulls to a stop, and to restart it when the driver accelerates. A reinforced starter is able to ensure this new function in addition to the classical cold start. Then, its life time has to be widely increased in comparison with a classical starter. They have to be optimized, and more especially their process of commutation in order to minimize commutator and brush wears, and thereby increase the lifetime of the device up to the whole life of the vehicle. The main contribution of the paper is the development of a coupled FE-circuit model taking into account local saturation and arc phenomena. Brush-segment contact resistance introduced in the circuit model has been computed efficiently and compared to measures. The whole model has been validated by experimental measurements which are carried out with specific experimental test benches.

1. INTRODUCTION

In order to answer the new European standards for fuel economy and reduction of greenhouse gas emissions, the automotive industry proposes technologies which are more respectful of the environment. They have been classified in three levels: full-hybrid, mild-hybrid and micro-hybrid which is also known as stop-start system. The present paper focuses on the last one. Such electromechanical conversion has the capability of energy recovery allowing the reduction of fuel consumption. This function can be provided by a starter-generator or even just a reinforced starter. The starter-generator system has been studied and tested in many situations in both electric vehicles and aerospace applications [1–5]. Such electromechanical conversion has the capability of energy recovery allowing the reduction of fuel consumption. Different topologies of stator windings can be used in order to increase the compactness of such devices [6, 7]. Actually, the development and study of a stop-start starter require detailed study of commutation phenomena. A bad commutation is harmful in terms of performance and also in terms of brush wear [8], which is directly related to the lifetime of the starter. The latter presents an electrical wear due to electrical arcing, and a mechanical wear proportional to the number of cycles made by the starter. The modeling of arcs in brushed starters is then essential to extend the expected life of these devices.

Nowadays, it is said that modeling DC machines attracts little interest when it is considered such as RLE circuit. However, if the model has to take into account commutation, arcs and local saturation of the armature, the problem becomes more interesting and difficult to carry out. Several kinds of models can be used. For example, we can use a model where the circuit inductance and no-load EMF are computed by finite elements [9–14]. This kind of models has the advantage of being fast. However, saturation of iron core and magnetic coupling between field system and armature coils are phenomena

Received 14 January 2014, Accepted 14 February 2014, Scheduled 28 March 2014

* Corresponding author: Julien Fontchastagner (julien.fontchastagner@univ-lorraine.fr).

¹ Université de Lorraine, GREEN, EA 4366, Vandœuvre-lès-Nancy F-54500, France. ² Valeo Electrical Systems, Ville Nouvelle de l'Isle d'Abeau, St Quentin Fallavier 38291, France.

which are not correctly taken into account with such models. Skin effect in DC motors with solid iron pole shoes is not considered at all. In this paper, a circuit-field coupled model is proposed with a time step solving of both circuit and field equations. This kind of models is available in some finite element software products and allows consideration of all the magnetic phenomena difficult to model so far. Therefore, the main contribution of this paper consists in the implementation of a model which takes into account the Brush-segment contacts thanks to switches and variable resistors [15]. A model of the electric arc is also implemented.

2. MODELING OF THE BRUSHED DC STARTER

In the first approach, the simulation of machines with mechanical commutator can be based on a model which neglects the phenomenon of commutation which is then studied separately. This kind of modeling is sufficient to have an overview of the behavior of the machine when it is supplied with a DC voltage. However, the modeling of the commutation phenomenon is essential to preventing the damage of the brush-commutator system.

2.1. Equivalent Circuit of the Starter

DC machines are composed of a field system in the stator (which is wound) and armature coils sections connected in series by the brushes-segment system. The role of the brushes is to supply armature sections with alternating current so that the field created by the armature is orthogonal to the field created by the coils in order to maximize the magnetic coupling. The general circuit is represented Figure 1.

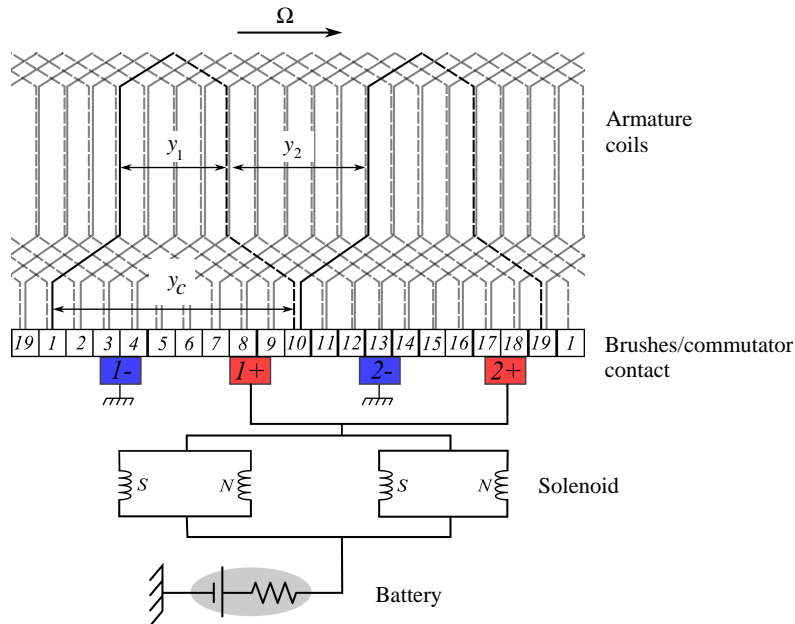


Figure 1. Global circuit representation of a 4 wound field poles and 4 brushes DC motor; relevant parameters of the armature winding.

The positions of brushes on the commutator determine the electrical behavior of armature sections. It is possible to know, for each mechanical position of the rotor, which segments are covered by brushes; this is illustrated in Figure 2. For our common range of brush and segment width ratio which are respectively called α and β on Figure 3, where N_s is the number of segments, two or three segments in contact with a brush can occur at the same time.

A Brush-segment electrical contact will be modeled as a resistive voltage drop called V_{a_i} and V_{c_i} in Figure 4 for the voltage drops respectively under the anodic brushes and the cathodic brushes. Knowing

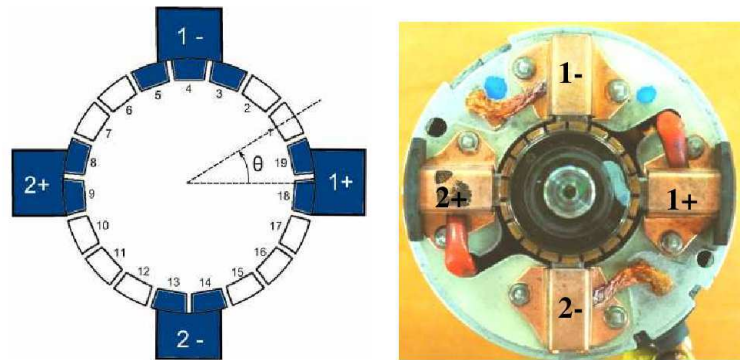


Figure 2. Representation of brushes/commutator contacts for a 4 brushes and 19 segments starter.

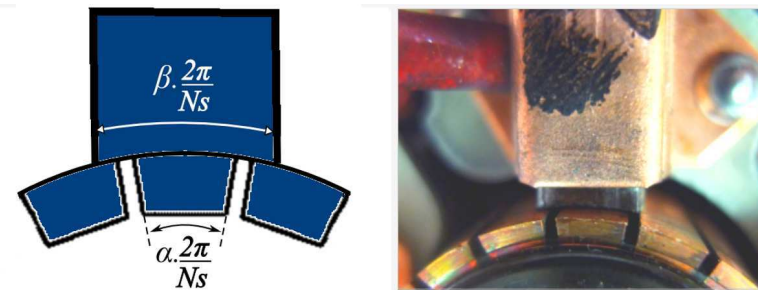


Figure 3. Segments of commutator covered by a brush. Relevant geometric parameters illustrated.

the structure of the armature winding (especially the commutator pitches y_c), it is possible to determine which sections are commuting under the anodic and cathodic brushes respectively represented by the $N1$ voltages ($U_{r1}, U_{r2}, \dots, U_{rN1}$) and the $N2$ voltages ($U_{rN1+1}, \dots, U_{rN1+N2+2}$) in the Figure 4. Finally the two remaining voltages U_{rN1+1} and $U_{rN1+N2+2}$ represent the two main paths (called “path+” and “path-”) made by armature coils in series. The equivalent electrical circuit can thus be determined for each rotor position.

2.2. The Brush-Segment Contact

The characterization of the electrical Brush-segment contact is certainly the most difficult point in the modeling of the starter. Many authors have already proposed different kinds of contact modeling [10–16].

Generally, the voltage drop between a brush and a segment is modeled by a variable resistance due to two phenomena: the resistance of the brush body and the voltage drop at the sliding interface.

These two elements are Brush-segment common surface contact dependent. Considering the α and β coefficients that respectively represent the segment width ratio and the brush width ratio as shown on Figure 3, we can build the ΔS function as the common surface between a brush and a segment. This function is characterized by three parts as shown in Figure 5 (the total mechanical contact equals to $(\alpha + \beta) \times 2\pi/N_e$, and a constant step exists when $\beta > \alpha$).

Knowing the ΔS value at each position for each Brush-segment contact, the aim is to build the equivalent contact resistance. Some authors use a conductance model proportional to the ΔS value [17, 18]. This model is rather good in a first approach but not accurate enough because it considers the current lines to be orthogonal to the contact; the current distribution is more complex in real conditions. Moreover, the brush can be made with anisotropic resistivity material [19] or with multi-layers. In automotive starter applications, brushes shown on Figure 6 are made with two layers of electric resistivity ρ_1 and ρ_2 in order to increase contact resistance at the end of the commutation and thus reduce arc occurring.

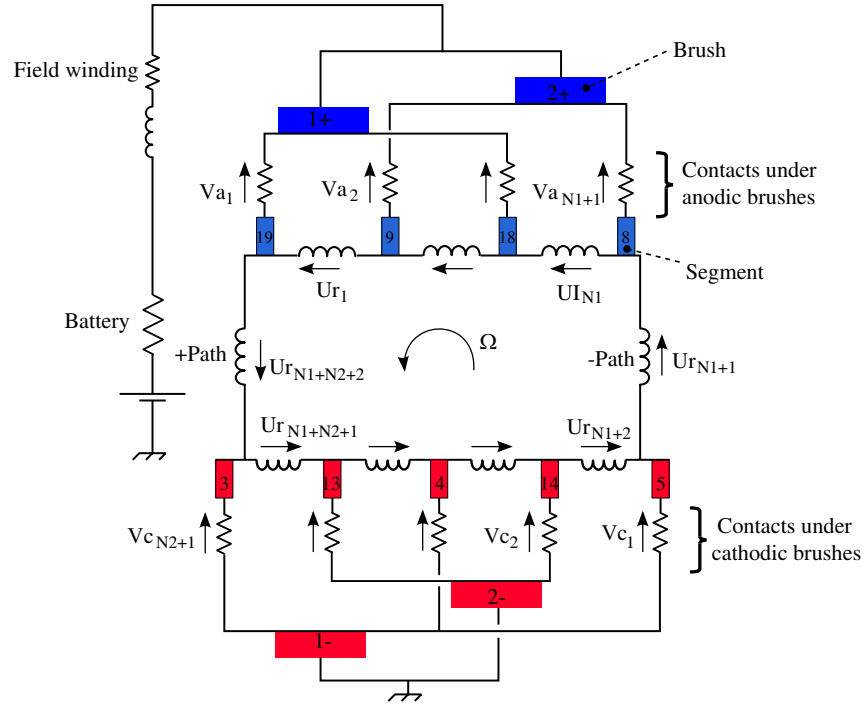


Figure 4. Equivalent electrical circuit of the armature represented in Figure 1 for the specific position of the brushes on the commutator represented on Figure 2 (the anodic brushes are in contact with the segments number 8-9-18-19 when the cathodic ones are in contact with the segments 3-4-5-13-14).

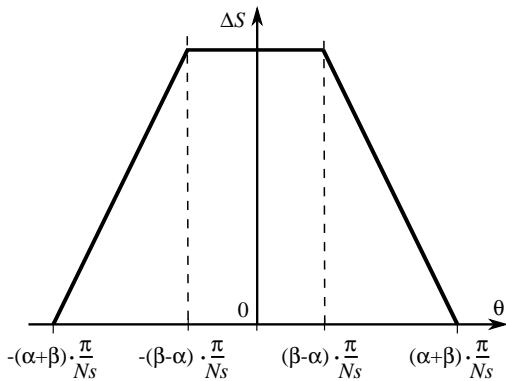


Figure 5. A Brush-segment common surface ΔS evolution with the position.

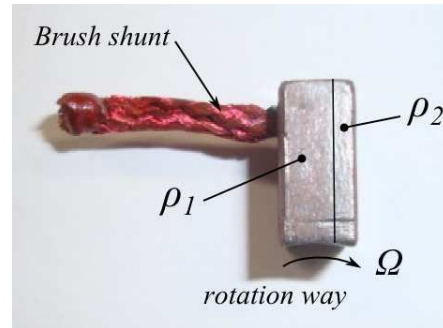


Figure 6. Double layer composition of a brush used in a car starter.

In the following, we propose a measurement method to characterize the electrical contact resistance which is a function of the position θ . We also develop a numerical approach using the finite element method.

2.3. Measurement of the Electrical Behavior of the Brush-Segment Contact

Generally, the main difficulty consists in the identification of lumped parameter of the model which combines many physical phenomena [20]. The measurement of such a sliding contact is difficult and not common in the literature. Authors often try to characterize the electrical behavior of a brush-ring sliding contact typically for synchronous machine applications [21, 22]. In the case of commutator machines, it is much more complex than a basic brush-ring contact, because the current and the contact surface

between the brush and the segment continuously evolve. We develop a specific device with a blank commutator composed of 19 segments mounted on a shaft. Segments are connected in order to form two isolated groups, and two brushes are connected to a DC source. Subsequently, the shaft is driven at constant speed with an auxiliary motor allowing two conducting periods per mechanical revolution. The device and its principle can be seen in Figure 7. A system with an external brush-ring allows monitoring the Brush-segment voltage drop ($U_1 - U_2$) while the contact is sliding. The current is also measured thanks to a Hall effect sensor. Finally, the total contact resistance (in the brush body and in the interface) is deduced as the ratio of the instantaneous voltage and current.

The aim of such a device is to measure the contact resistance versus the θ value; the use of the term of “resistance” suggests the behavior to be independent of the contact current. However, the layer located between the brush and the segment, and composed of a mixture of copper oxide and carbon dust, has a non-linear behavior.

Measurements of the device have been carried out with two different values of the current (I_0 and $3I_0$) as shown on Figure 8. Although the current is three times bigger, the obtained voltage drop ($U_1 - U_2$) waveforms are not linked by the ratio 3. This refers to a non-linear behavior. The measurements show that the voltage drop increases with a factor greater than 10 between a full contact ($\theta = 0^\circ$) and just before the end of the mechanical contact when $\theta = (\alpha + \beta) \times 360/N_e$. The device can only display electrical behavior of the second part of the contact where $\theta > 0^\circ$.

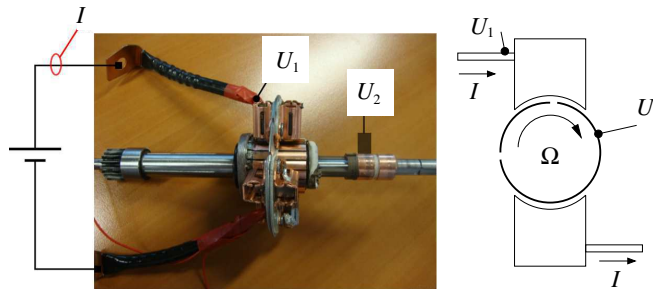


Figure 7. Specific test bench and principle of the Brush-segment sliding contact resistance measurement.

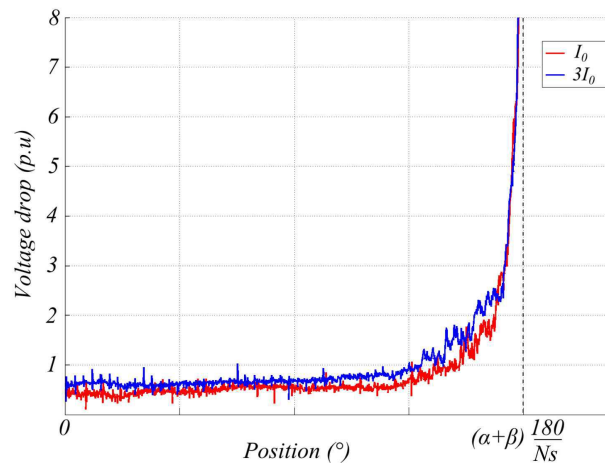


Figure 8. Electric measurements of the brush-commutator sliding contact when $\theta > 0^\circ$.

2.4. Modeling of the Brush-Segment Contact

For more accuracy, a finite element model using current flow equations can be used to identify the equivalent contact resistance (see Figure 9). A similar numerical approach has been used for the study

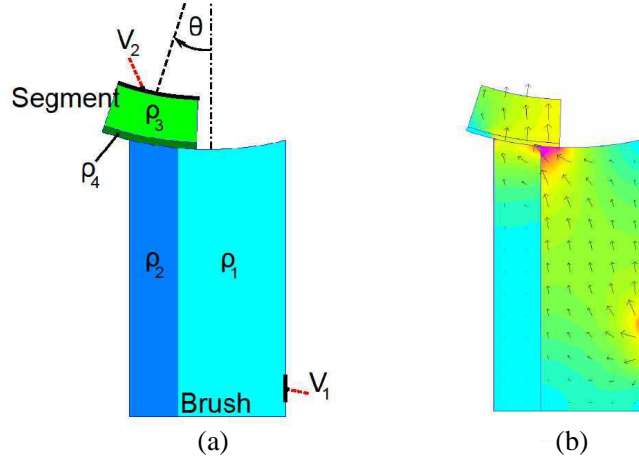


Figure 9. Current flow F.E. model for Brush-segment contact resistance and example of current density for an imposed position θ .

of brush body resistance for universal motors where carbon brushes are employed [10–19]. Authors have noticed the importance of considering the current flow between segments located under the same brush. The voltage drop at the interface is often added using an analytical expression regarding the contact area ΔS as in [10] or the current density as in [11]. Regarding measurements made in Figure 8, we can say that the total voltage drop (i.e., in the brush body and at the interface) mainly depends on the contact area in our application.

Moreover, it is well known that the voltage drops are different under anodic or cathodic brushes. We will neglect this phenomenon in the following.

Thus, the distribution of current density in the brush is complex because of the use of double-layered brushes (shown on Figure 6), and a Finite Element model seems more relevant. We propose to identify the equivalent contact resistance using current flow computation. The voltage drop at the sliding contact is also integrated in our numerical approach by considering a highly resistive thin layer at the contact ($\rho_4 \gg \rho_3$) as showed in Figure 9. The ρ_4 resistivity is chosen to correlate our model with measurements as shown on Figure 10.

The F.E. computation of the current flow is based on a scalar potential formulation. The current density J (see Figure 9) is obtained from differentiation of the field of potential. The two surfaces represented with black lines are considered as two Dirichlet boundary conditions, respectively with V_1 and V_2 voltages. The V_1 potential is related to the potential of the brush cable and the V_2 potential at the bottom of a segment.

Resistance is finally deduced from the Finite Element calculation of the electrical power W using the definition:

$$W = l_{br} \sum_i \rho_i J_i^2 S e_i \quad (1)$$

where:

- l_{br} is the axial length;
- J_i is the current density in the i th element of the mesh;
- ρ_i and $S e_i$ are respectively the electric resistivity and the surface of the i th element.

In order to validate this model, experimental measurements have also been carried out to determine a resistance of a Brush-segment which depends on the position. The test bench presented in the previous section allows to determine the equivalent resistance for a given geometry. Figure 10 shows the results of the measurement (blue) and those provided by finite element model (red).

Model and measurement show a significant increase of the resistance at the end of mechanical contact. It may be noticed that this resistance is multiplied by ten comparing the “full” contact and the end of mechanical contact, just before the electrical arc.

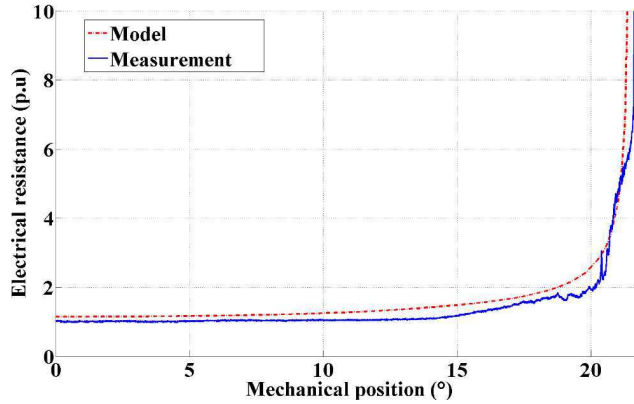


Figure 10. Evolution of a Brush-segment contact resistance with the relative position of the segment calculated by the F.E. model (red) and measured (blue).

In the following, we will assume that the current through the Brush-segment is relatively constant during the real operation of the starter. It means that we can consider the electrical contact as purely resistive and use the numerical model as previously described. This assumption will be discussed in a next section.

2.5. Modeling of the Arc

At the end of the mechanical contact, when the segment leaves the brush, an arc occurs until the total extinction of the current. In this case, an arc voltage is added to the ohmic drops in the brush and the segment. This voltage (2) depends on the arc current (I_a) and also the length of the arc (e_a). Several authors have proposed models for the arc [10, 11, 16]. We adopt an “external” model as the “Ayrton” model that involves the arc length and intensity. This semi-empirical model (2) is suitable to be implemented into a circuit model.

$$U_{arc}(I_a, e_a) = A + \frac{B}{I_a} + C e_a + D \frac{I_a}{e_a} \tag{2}$$

By ignoring constant and the D coefficient, we consider the following simplified model:

$$U_{arc}(I_a, e_a) = \frac{B}{I_a} + C e_a \tag{3}$$

And the two coefficients (B and C) of (3) are determined empirically.

3. IMPLEMENTATION OF THE MODEL IN A FIELD-ELECTRIC CIRCUIT COUPLED MODEL

3.1. Introduction

Strong coupling models combine field equations with those of the electrical circuit in the same differential system [23]. Time stepping finite element are widely used for the study of brush less DC motors [24], induction motor [25–28], or current transformers [29]. However, switching model for brushed DC motor remains complex and unusual. Various software (Flux2D, ANSYS Maxwell, Opera-2d . . .) provide this feature that facilitates the user’s work [16, 17, 30]. We have developed an approach using the FLUX2D software in batch mode controlled with a Python code to model the switch as defined at the previous section. The main program uses the results of the previous iteration to determine the state of the circuit at the current time and provide the appropriate values of contact resistances and arc voltage. The principle of the algorithm is described in Figure 11.

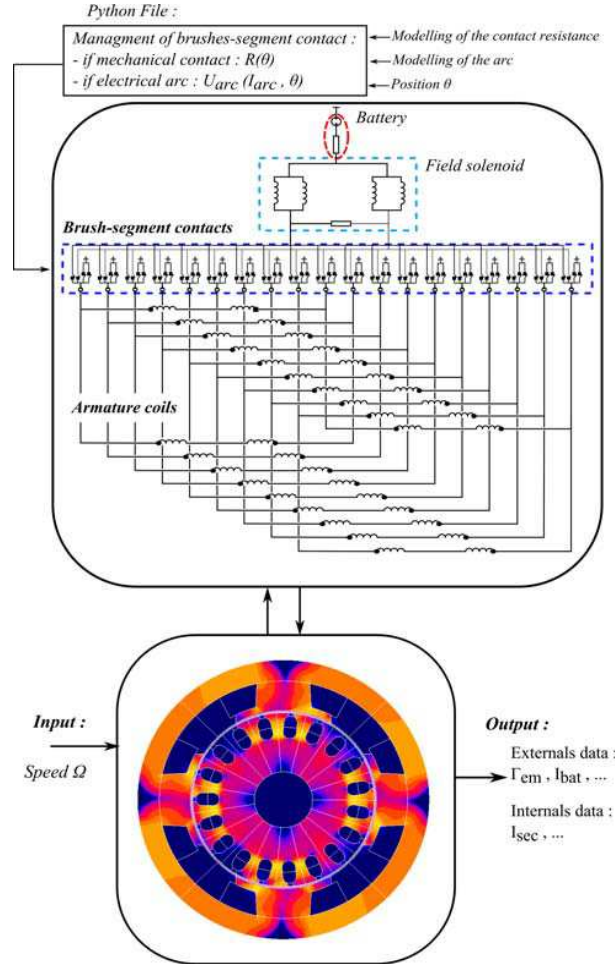


Figure 11. Description of algorithm with magnetic/electric coupling.

3.2. Resolution and Mesh Description

We solve a transient magnetic time-stepping problem coupled to an electrical circuit at constant speed. The electrical equation solved is:

$$[\mathbf{V}] = [\mathbf{R}_c] \cdot [\mathbf{I}] + \Omega \frac{\partial}{\partial \theta} [\Phi] \quad (4)$$

where $[\Phi]$ is the flux vector computed by the finite element software in each coil; $[\mathbf{V}]$ and $[\mathbf{I}]$ are the voltage and current vectors of the circuit branches; $[\mathbf{R}_c]$ is the resistance matrix of the circuit.

The speed Ω is assumed to be constant. The angular step $\Delta\theta$ has to be adapted to the size of the mesh in the rotating air gap. Authors have already studied movement for field computations in such situation [31], and the moving band method is used here [32]. This step must be connected to the size of an element in the air gap in order to limit numerical instabilities (in particular for the calculation of electromagnetic torque) due to mesh noise. The mesh description of the entire machine is shown in Figure 12 and in Figure 13 for the air gap. Mesh in the stator must be particularly refined to take into account eddy currents in the solid iron pole shoes.

3.3. Implementation of the Brush-Segment Contact Resistance and the Arc Voltage in the Coupled Circuit

As mentioned in the previous section, the knowledge of the equivalent resistance on voltage drop is essential for the study of commutation. The Brush-segment contacts are modeled in the circuit by

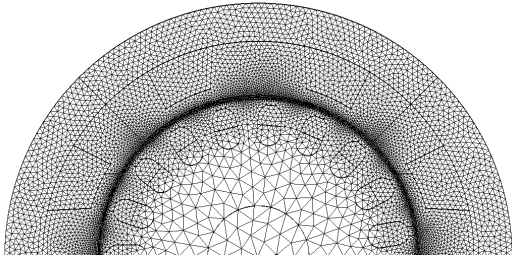


Figure 12. Description of the mesh in the entire machine.

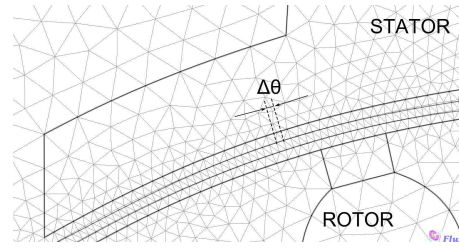


Figure 13. Description of the mesh in the air gap.

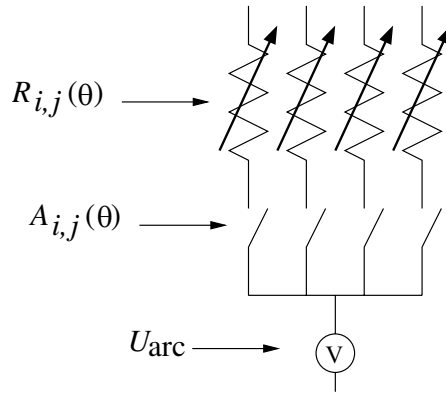


Figure 14. View of the brushes-segment and arc component.

$N_b \times N_s$ switches as shown on Figure 14 where N_b and N_s are respectively the number of brushes and segments. We isolate in Figure 10 the model of one segment contact with the N_b brushes.

The switch-on/switch-off orders of the switches are represented by the $[\mathbf{A}(\theta)]$ matrix given in (5). This matrix of N_b rows and N_s columns contains only 0 or 1 and defined as follows:

$$A_{i,j}(\theta) = \begin{cases} 1 & \text{if the segment } j \text{ is situated under the brush } i \\ 0 & \text{otherwise} \end{cases} \quad (5)$$

Note that the matrix $[\mathbf{A}(\theta)]$ can only contain one “1” per column.

Switch resistances are located in a matrix also depending on the position, written $[\mathbf{R}(\theta)]$. The current term of this matrix is calculated according to the mutual surface between the brush i and the segment j . The relation between resistances and surfaces has already been developed in the previous section. Finally, every term $R_{i,j}$ of the resistance matrix $[\mathbf{R}(\theta)]$ can also be expressed from a single term $R_{1,1}(\theta)$ as in (6); the other terms are obtained by circular permutation. The $R_{1,1}(\theta)$ term has been calculated and measured and shown on Figure 7.

$$R_{i,j}(\theta) = R_{1,1} \left(\theta - (j - 1) \frac{\pi}{p} + (i - 1) \frac{2\pi}{N_s} \right) \quad (6)$$

When no mechanical contact exists and if the current in the related coil is not totally reversed, an arc can occur at the brush trailing edge. In such situation an additional arc voltage is added to the model in series with the corresponding switch. The switch is then stuck in the “closed” position and an arc voltage is added to the contact resistance until the arc vanishes, i.e., the current in the coil is equal to the current in the main path considered (the currents comparison is ensured by the algorithm). The arc voltage characteristic has been explained in the previous section.

4. RESULTS, DISCUSSIONS AND COMPARISON WITH MEASUREMENTS

4.1. Description of the Test Bench

Direct measurements of armature current during rotation in brushed DC motors are often made [8, 10]. In most cases, it concerns high voltage/low current motor so that two slip rings with brushes are used to exit one coil current while the armature is rotating as illustrated on Figure 15. Current can thus be measured thanks to a Hall effect sensor. In the case of a car starter, this technique is much more difficult to carry out because of the low resistance of the armature coils compared to the additional resistance of the two slip rings connected in series. In our specific armature, we use 4 copper composition brushes in parallel per sliding ring in order to have a sliding contact resistance as smaller as possible. All the others coils of the armature are also designed (with a smaller inner copper diameter) to have an armature winding electrically balanced (same resistance per section). The developed armature also enables the measurement of the potential of the two segments (called V_1 and V_2) located at the bottom of the considered coil as shown on Figure 15. Finally, the device allows the knowledge of all of the internal waveforms (coil current and voltage, Brush-segment voltage drop) characterizing the commutation phenomena.

The prototype, shown on Figure 16, is driven at constant speed with an external motor and supplied by a 12 V voltage source. The brushes and the armature used on the device have been run in before the measurements in order to have a good shape of the brushes and a good commutator film quality.

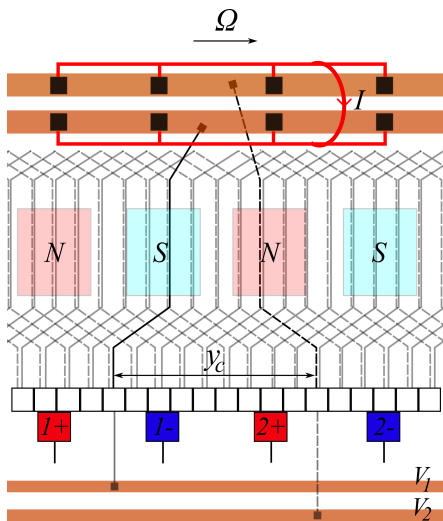


Figure 15. Principle of measurement of the internal waveforms.



Figure 16. Prototype with slip rings for internal measurements.

4.2. Comparison of the Model with Measurements

Results of the previous model can be compared to measurements thanks to the specific test bench. We are going to compare coil current waveforms (Figure 17) and Brush-segment voltage drop waveforms (Figure 18) for one operating point (6000 rpm) and a negative brush shift angle (-5 mechanical degrees) during one mechanical revolution.

We first observe that both waveforms are relatively close to measurements especially in terms of amplitude. However, we can notice that the calculated current waveform (Figure 17) does not fit to the measured one during the commutation process. The model predicts a reverse phenomenon of the current appearing approximately at the middle of the commutation which has not been observed at all in practice. This reverse phenomenon corresponds to when the current that flows in the contact (Figure 19) is negative. It means that the purely resistive model used does not fit here because the brush to segment current is not constant at all during the commutation process as assuming previously.

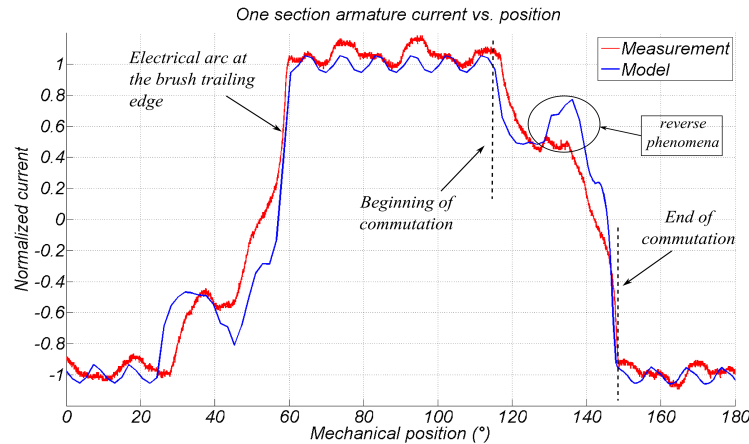


Figure 17. Current waveforms during one electrical period obtained by measurement (red) and by calculation (blue) at the speed of 6000 rpm.

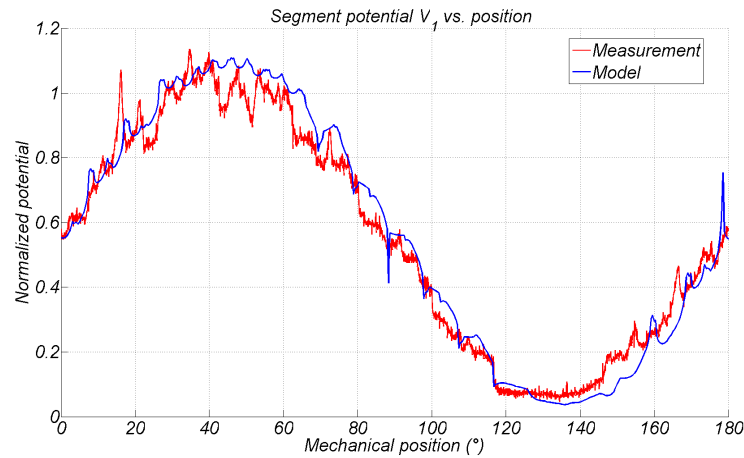


Figure 18. Positive brush-to-segment voltage waveforms in one electrical period obtained by measurement (red) and by calculation (blue) at the speed of 6000 rpm.

In the following, we will propose a new electrical model for the brush to segment sliding contact to improve the model versus the measurements and consider the non-linearity of the electrical contact.

4.3. Improvement of the Sliding Contact Model

It consists in taking into account the non-linearity of the contact that has previously been highlighted thanks to specific measurements (Figures 7 and 8). We introduce a current dependency when calculate the resistance of a brush to segment contact. For example, we can use the simple low given in Figure 20. Knowing the value of the current that flows in the contact during the previous position, we deduce the ratio to apply the resistance r_{sat} calculated as previously explained (regarding the ΔS common surface between the brush and the segment). In this case, the ratio is comprised between one and three. This new model still does not make difference between anodic and cathodic contact (which can also be differentiated by the sign of the current that flows in the contact).

The procedure of the non-linear resistance achieving is described on Figure 21. The others steps remain the same as previously.

We compare, in Figure 22, current waveforms obtained by the model using the pure resistive contact resistance and the new approach previously given for a speed of 6000 rpm and a positive brush shift angle

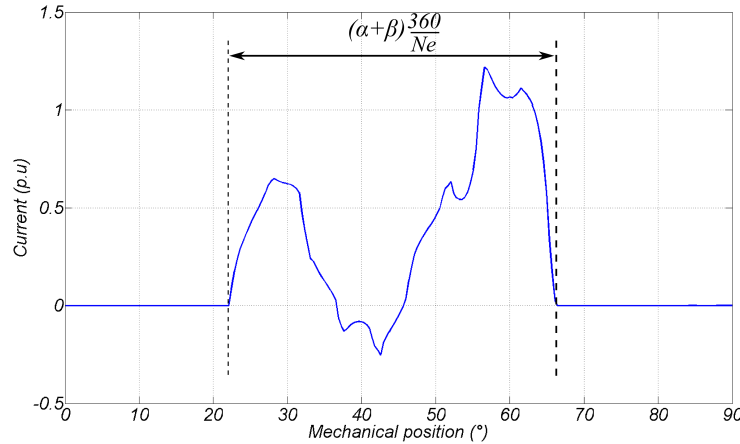


Figure 19. Current waveform in one brush-to-segment contact obtained numerically.

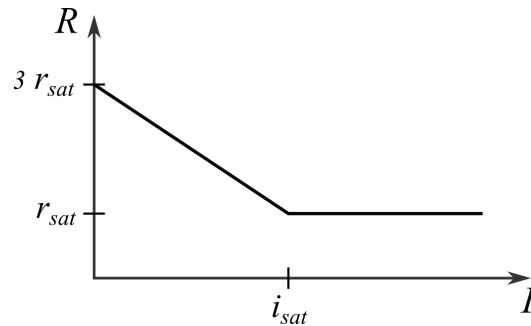


Figure 20. Non-linear electrical contact model.

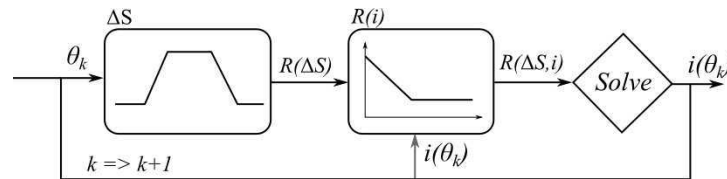


Figure 21. Scheme for contact resistance achievement.

of $+1^\circ$. In practice, such a positive angle is disallowed to limit arc production. Both resistance models (the purely resistive and the non-linear ones) are compared here because the “reverse” phenomenon observed during the commutation in the current waveform is particularly present for positive brush shift angles. We observe that the amplitude of the phenomenon is divided by three when comparing the purely resistive model (ΔI_2) and the non-linear model adopted ($\Delta I_1 = \Delta I_2/3$).

4.4. Improvement of the Commutation Phenomena

The developed model provides, with a good accuracy, the knowledge of internal variables especially during the commutation process. Some direct measurements allowed taking a critical look on the developed model. We can now use this approach to improve the commutation behavior of our device by adjusting some build parameters such as the brush width or the brush shift angle.

We can first search the effect of the brush width on the commutation and performances. The duration of the commutation is proportional to this parameter. With a same brush shift angle, it is possible to use a greater width of the brushes to start the commutation sooner and thus help the

inversion of the current (thanks to a greater E.M.F induced in the section). We have made simulations with three different brush widths to segment width ratios at the same speed: 1, 1.4 and 1.8. Current waveforms are displayed on Figure 23.

We note that the arc at the end of the commutation process is approximately the same in the three studied cases. Regarding the numerical results, we can say that the benefit of having a larger brush width (i.e., a longer commutation duration) is not significant. Moreover, it is also not beneficial for the electromechanical conversion. Results are displayed on the Table 1; average battery currents and electromagnetic torques are expressed in per units which refers to the 1.4 brush width ratio.

We observe that the 1.8 brush width ratio case leads to the same level of torque with a current level increase by 7% which is harmful for the electromechanical conversion. The 1.0 brush width ratio has the best static performance but such a ratio is too small to ensure good stability of the brush on the commutator.

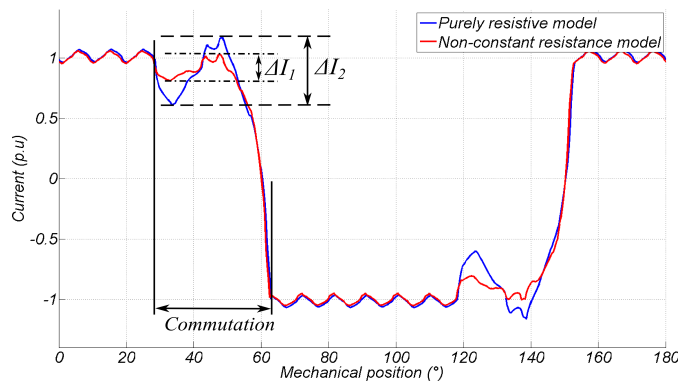


Figure 22. Current waveforms at the speed of 6000 rpm and with a brush shift angle of $+1^\circ$ obtained with the purely resistive model (blue) and the non-constant resistive model (red).

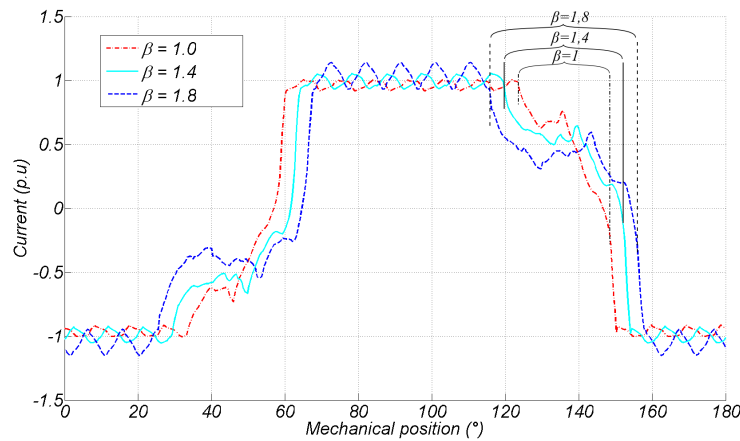


Figure 23. Effects of the brush width on the armature coil current waveform especially during the commutation.

Table 1. Relevant data for the brush width effect.

| Brush width ratio β | 1.0 | 1.4 | 1.8 |
|-----------------------------------|------|------|------|
| Commutation duration ($^\circ$) | 25.8 | 33.3 | 40.9 |
| Battery current (p.u.) | 0.99 | 1.00 | 1.07 |
| Electromagnetic torque (p.u.) | 1.06 | 1.00 | 1.00 |

5. CONCLUSION

This paper deals with the modeling of brushed Starter for a micro-hybrid system in automotive application. The main objective is to have an accurate model which takes into account many phenomena such as contact resistance of the brush-commutator, local saturation and electric arcs. The model uses a finite element calculation of electromagnetic fields in the armature and current flow in the brushes. It is based on a strong coupling with the circuit model taking into account the Brush-segment contact and the electric arc that occurs at the end of the commutation phase.

The model of the contact resistance based on current flow equations in the brush-commutator system is validated with experimental measurements on a specific test bench. In addition, a prototype has been constructed to make the measurement of the current in a rotor section possible during the normal operation of the DC starter. These experimental results validate the coupled model developed in this paper.

This model can be used as a designing tool to improve starter behavior through modifying the commutation process and minimizing the arc amplitude at the brush trailing edge. The use of this model in a multi-objective optimization process requires a reduction of CPU time (of the fitness or constraints functions) which is not recommended here. However a parametric variation process using static performances can give a best structure of the motor. And then, the coupled model can be a posteriori used to study deeply the transient behavior of the starter. Such complementarity of models is very beneficial for improving the performances of complex systems.

REFERENCES

1. Griffo, A., D. Drury, T. Sawata, and P. H. Mellor, "Sensorless starting of a wound-field synchronous starter/generator for aerospace applications," *IEEE Trans. Ind. Electron.*, Vol. 59, No. 9, 3579–3587, 2012.
2. Chen, Z., H. Wang, and Y. Yang, "A doubly salient starter/generator with two-section twisted-rotor structure for potential future aerospace application," *IEEE Trans. Ind. Electron.*, Vol. 59, No. 9, 3588–3595, 2012.
3. Wang, C.-F., M.-J. Jin, J.-X. Shen, and C. Yuan, "A permanent magnet integrated starter generator for electric vehicle onboard range extender application," *IEEE Trans. Magn.*, Vol. 48, No. 4, 1625–1628, 2012.
4. Seo, J.-H., S.-M. Kim, and H.-K. Jung, "Rotor-design strategy of IPMSM for 42 V integrated starter generator," *IEEE Trans. Magn.*, Vol. 46, No. 6, 2458–2461, 2010.
5. Chai, F., Y. Pei, X. Li, B. Guo, and S. Cheng, "The performance research of starter-generator based on reluctance torque used in HEV," *IEEE Trans. Magn.*, Vol. 45, No. 9, Part 1, 2458–2461, 2010.
6. Fukami, T., Y. Matsuura, K. Shima, M. Momiyama, and M. Kawamura, "A multipole synchronous machine with non-overlapping concentrated armature and field windings on the stator," *IEEE Trans. Ind. Electron.*, Vol. 59, No. 6, 2583–2591, 2012.
7. Di Stefano, R. and F. Marignetti, "Electromagnetic analysis of axial-flux permanent magnet synchronous machines with fractional windings with experimental validation," *IEEE Trans. Ind. Electron.*, Vol. 59, No. 6, 2573–2582, 2012.
8. Pavlovcic, F., "The commutator optimization due to electrically caused wear," *Proc. XIX International Conference on Electrical Machines (ICEM'2010)*, 1–6, Sep. 6–8, 2010.
9. Vauquelin, A., J.-P. Vilain, S. Vivier, N. Labbe, and B. Dupeux, "A new modeling of DC machine taking into account commutation effects," *Proc. XVIII International Conference on Electrical Machines (ICEM'2008)*, 1–6, Villamoura, Portugal, Sep. 6–9, 2008.
10. Wang, H., "Modeling of universal motor performance and brush commutation using finite element computed inductance and resistance matrices," *IEEE Trans. Energy Convers.*, Vol. 15, No 3, 257–263, 2000.
11. Di-Gerlando, A. and R. Perini, "Model of commutation phenomena in a universal motor," *IEEE Trans. Energy Convers.*, Vol. 21, No. 1, 27–33, 2006.

12. Batzel, T. D., N. C. Becker, and M. Comanescu, "Analysis of brushed dc machinery fault with coupled finite element method and equivalent circuit model," *IJME*, Vol. 11, No. 2, 5–13, 2011.
13. Matsuda, T., T. Moriyama, N. Konda, Y. Suzuki, and Y. Hashimoto, "Method for analyzing the commutation in small universal motors," *IEE PROC-B*, Vol. 142, 123–130, 1995.
14. Glowacz, Z. and W. Glowacz, "Mathematical model of dc motor for analysis of commutation processes," *EPQU*, Vol. 8, 65–68, 2007.
15. Andreux, R., J. Fontchastagner, N. Takorabet, N. Labbe, and J-S. Metral, "Magnetic field-electric circuit coupled method for brush DC motor simulations," *Proc. XXth International Conference on Electrical Machines (ICEM'2012)*, Marseille, France, Sep. 2–5, 2012.
16. Sincero, G. C. R., J. Ghannou, J. Cros, and P. Viarouge, "Collector model for simulation of brush machines," *Math. Comput. Simulation*, Vol. 81, 340–353, 2010.
17. Lin, D., P. Zhou, W. N. Fu, B. Ionescu, and Z. J. Cendes, "Flexible approach for brush-commutation machine simulation," *IEEE Trans. Magn.*, Vol. 44, No. 6, 1542–1545, 2008.
18. Sincero, G. C. R., J. Cros, and P. Viarouge, "Arc models for simulation of brush motor commutations," *IEEE Trans. Magn.*, Vol. 44, No. 6, 1518–1521, 2008.
19. Willing, M., T. Miller, and I. Corral, "A brush model for detailed commutation analysis of universal motors," *Proc. XXth International Conference on Electrical Machines (ICEM'2012)*, Marseille, France, Sep. 2–5, 2012.
20. Bracikowski, N., M. Hecquet, P. Brochet, and S. V. Shirinskii, "Multiphysics modeling of a permanent magnet synchronous machine by using lumped models," *IEEE Trans. Ind. Electron.*, Vol. 59, No. 6, 2426–2437, 2012.
21. Holzapfel, C., "Selected aspects of the electrical behavior in sliding electrical contacts," *Proc. IEEE 57th Holm Conference on Electrical Contacts*, 1–9, Sep. 2011.
22. Liu, K., Z. Q. Zhu, Q. Zhang, and J. Zhang, "Influence of non ideal voltage measurement on parameter estimation in permanent-magnet synchronous machines," *IEEE Trans. Ind. Electron.*, Vol. 59, No. 6, 2438–2447, 2012.
23. Fu, W. N. and S. L. Ho, "Extension of the concept of windings in magnetic field-electric circuit coupled finite-element method," *IEEE Trans. Magn.*, Vol. 46, No. 6, 2119–2123, 2010.
24. Liu, R., Y. Zhang, M. Hu, and D. Yan, "Field circuit coupled time stepping finite element analysis on permanent magnet brushless DC motors," *Proc. ICEMS 2005*, Vol. 3, 2105–2108, 2005.
25. Wang, X. and D. Xie, "Analysis of induction motor using field-circuit coupled timeperiodic finite element method taking into account of hysteresis," *IEEE Trans. Magn.*, Vol. 45, No. 3, 1740–1743, 2009.
26. Pusca, R., R. Romary, V. Fireteanu, and A. Ceban, "Finite element analysis and experimental study of the near-magnetic field for detection of rotor faults in induction motors," *Progress In Electromagnetics Research B*, Vol. 50, 37–59, 2013.
27. Akbari, H., "A modified model of squirrel cage induction machine under general rotor misalignment fault," *Progress In Electromagnetics Research B*, Vol. 54, 185–201, 2013.
28. Konwar, R. S., K. Kalita, A. Banerjee, and W. K. S. Khoo, "Electromagnetic analysis of a bridge configured winding cage induction machine using finite element method," *Progress In Electromagnetics Research B*, Vol. 48, 347–373, 2013.
29. Lesniewska, E., and R. Rajchert, "3D field-circuit analysis of measurement properties of current transformers with axially and radially connected cores made of different magnetic materials," *Progress In Electromagnetics Research M*, Vol. 28, 1–13, 2013.
30. Kurihara, K. and S. Sakamoto, "Steady-state and transient performance analysis for universal motors with appropriate turns ratio of lead coils to lag coils," *IEEE Trans. Magn.*, Vol. 44, No. 6, 1506–09, 2008.
31. Davat, B., R. Ren, and M. Lajoie-Mazenc, "The movement in field modeling," *IEEE Trans. Magn.*, Vol. 21, No. 6, 2296–2298, 1985.
32. Sadowski, N., Y. Lefevre, M. Lajoie-Mazenc, and J. Cros, "Finite element torque calculation in electrical machines while considering the movement," *IEEE Trans. Magn.*, Vol. 28, No. 2, 1410–1413, 1992.